The Charge-Time-Of-Flight Instrument

CELIAS Workshop - Göttingen

N. Janitzek, A. Taut, and L. Berger

Institut für Experimentelle und Angewandte Physik der
Christian-Albrechts-Universität zu Kiel

August 2014

Overview

1. CTOF
   - Principle of Operation
   - In-Flight Calibration $\rightarrow$ m/q algorithm
2. Heavy Pickup Ions
   - What are Pickup Ions
   - Interstellar Source of Pickup Ions
   - Inner Source of Pickup Ions
3. Heavy Pickup Ions - CTOF Observations
   - Inner Source Pickup Ions - CTOF
   - Short-Term Variability of the Inner Source
   - Composition of the Inner Source

CTOF - Principle of Operation

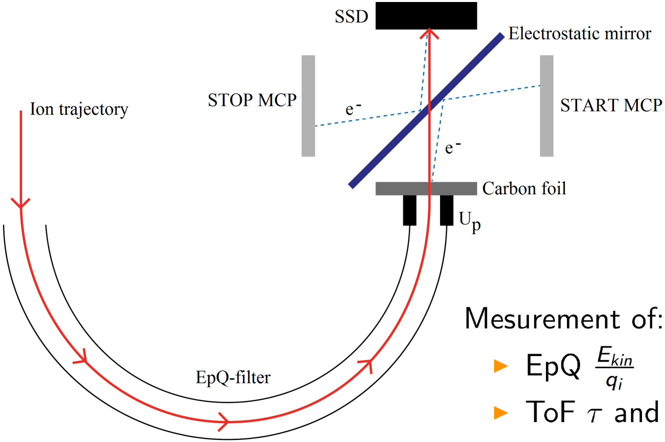

Mesurement of:

- EpQ $\frac{E_{kin}}{q_i}$
- ToF τ and
- Residual energy E_{SSD}.

CTOF - Principle of Operation

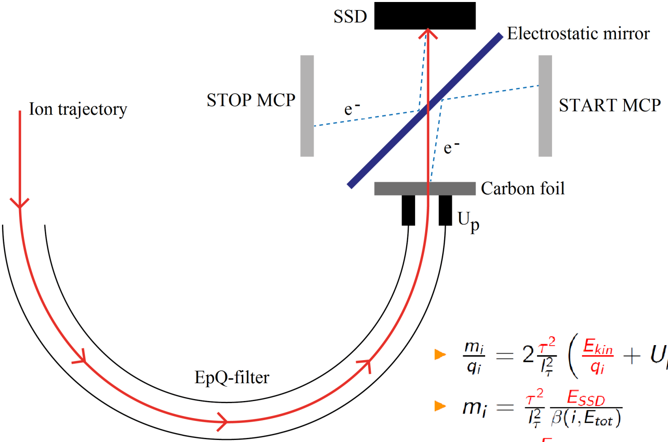

- $\frac{m_i}{q_i} = 2\frac{\tau^2}{l_\tau^2}\left(\frac{E_{kin}}{q_i} + U_p\right) \cdot \eta(i, E_{post})$
- $m_i = \frac{\tau^2}{l_\tau^2} \frac{E_{SSD}}{\beta(i, E_{tot})}$
- $E_{kin} = \frac{E_{kin}}{q_i} \cdot q_i$

In-Flight Calibration - Overview

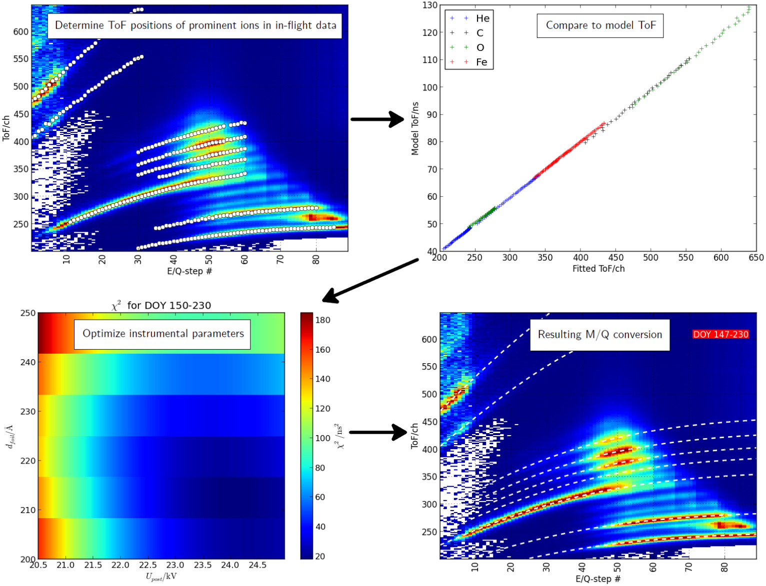

In-Flight Calibration - Overview

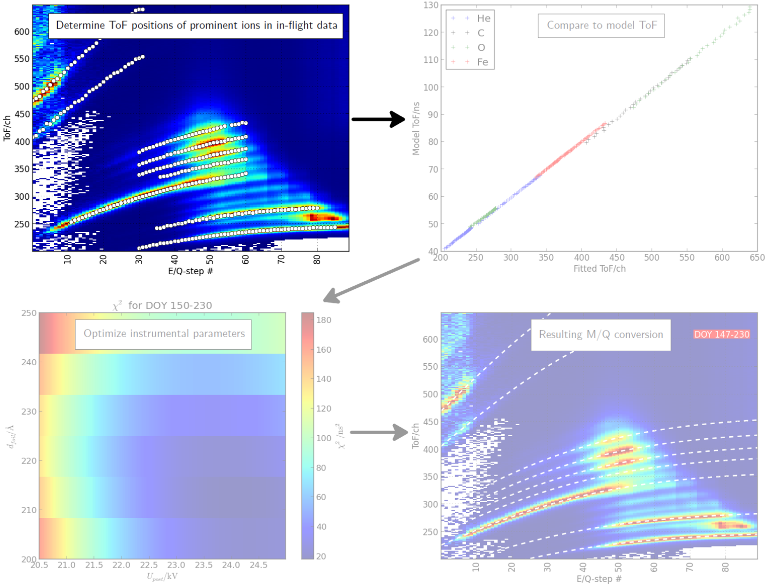

In-Flight Calibration

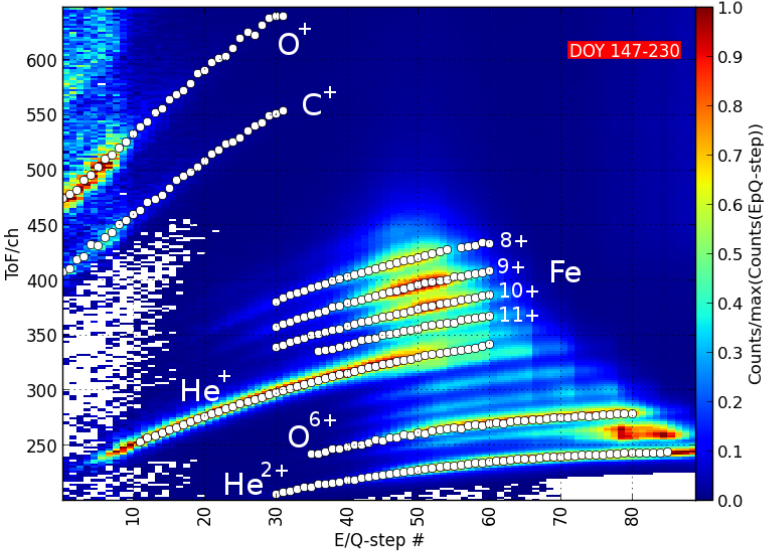

In-Flight Calibration

$$\boxed{\frac{m}{q} = 2\frac{\tau^2}{l^2}\left(\frac{E}{q} + U_p\right) \cdot \eta(i, E_{post})}$$

- $\eta(i, E_{post})$: Relative ToF delay due to energy deposition and angular scattering in the carbon foil
  $\rightarrow$ derived from TRIM simulations.
- Problem: no conversion from ch in ns given!

In-Flight Calibration

$$\frac{m}{q} = 2\frac{\tau^2}{l^2}\left(\frac{E}{q} + U_p\right) \cdot \eta(i, E_{post})$$

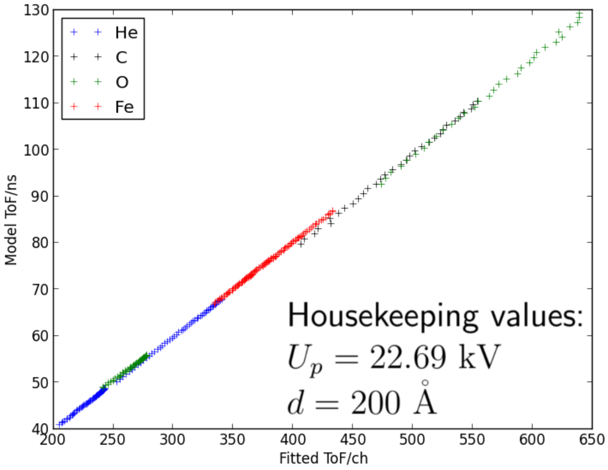

In-Flight Calibration

$$\frac{m}{q} = 2\frac{\tau^2}{l^2}\left(\frac{E}{q} + U_p\right) \cdot \eta(i, E_{post})$$

- $\eta(i, E_{post})$: Relative ToF delay due to energy deposition and angular scattering in the carbon foil
  $\rightarrow$ derived from TRIM simulations.
- Problem: no conversion from ch in ns given!

- Criterion: linear ToF conversion.
  $\rightarrow$ Minimize deviation of linear fit of ToF positions (in ch) vs. model ToF!
- Adapt model to in-flight data by optimizing U_p and foil thickness d.

In-Flight Calibration

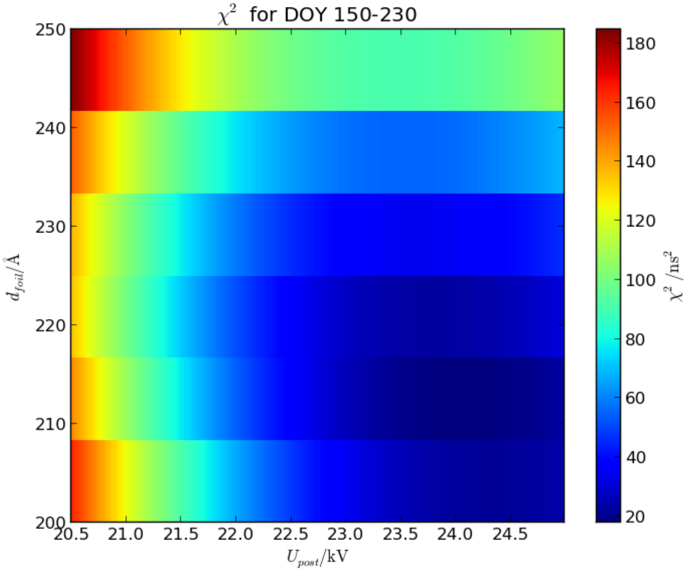

In-Flight Calibration - Result

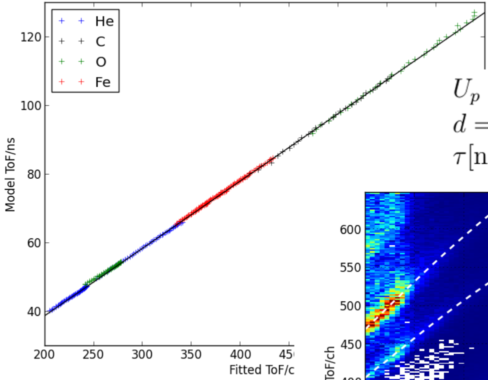

$$U_p = 24.07 \text{ kV}/20.04 \text{ kV}$$
$$d = 210 \text{ Å}$$
$$\tau[\text{ns}] = 0.197\frac{\text{ns}}{\text{ch}} \cdot \tau[\text{ch}] - 0.941\text{ns}$$

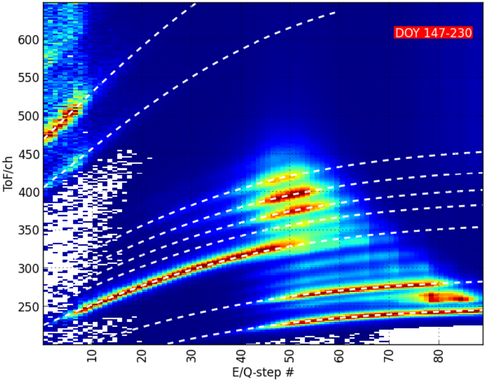

Heavy Pickup Ions

Pickup Ions

- What are Pickup Ions?
  - Not of (direct) solar origin
  - Embedded in the solar wind
- How can we identifiy Pickup Ions?
  - We can measure m_{ion}, q_{ion}, and v_{ion}
  - We can not measure the source!

Pickup Ions

- What are Pickup Ions?
  - Not of (direct) solar origin
  - Embedded in the solar wind
- How can we identifiy Pickup Ions?
  - We can measure m_{ion}, q_{ion}, and v_{ion}
  - We can not measure the source!

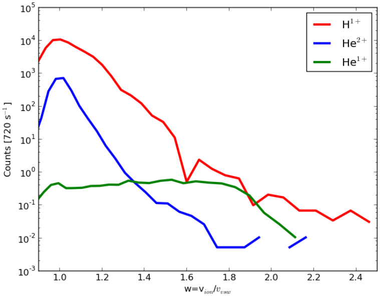

ACE/SWICS

Interstellar Neutral Gas

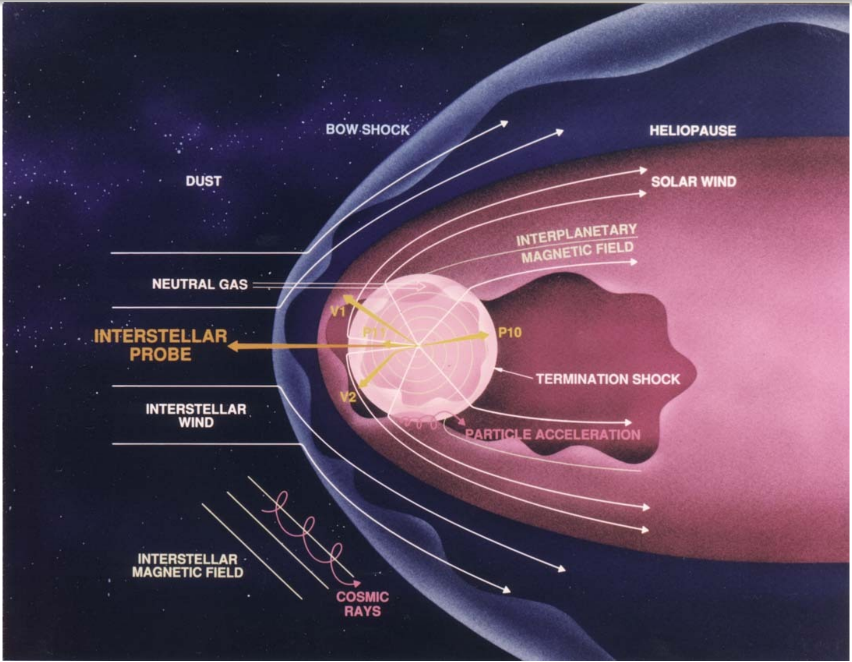

Interstellar Pickup Ions

Direct observation of He^+ pick-up ions of interstellar origin in the solar wind

E. Möbius*, D. Hovestadt*, B. Klecker*, M. Scholer*, G. Gloeckler† & F. M. Ipavich†

* Max-Planck-Institut für Physik und Astrophysik, Institut für extraterrestrische Physik, 8046 Garching, FRG
† Department of Physics and Astronomy, University of Maryland, College Park, Maryland 20742, USA

Singly-ionized helium with a velocity distribution extending up to double the solar wind velocity has been detected in interplanetary space. This distribution unambiguously determines the source: interstellar neutrals, ionized and accelerated in the solar wind. The observed significant flux increase in early December is due to the gravitational focusing of the interstellar neutral wind on the downwind side of the Sun.

THE penetration of the interstellar medium into the heliosphere and the interaction between the solar wind and the interstellar gas have been of great interest for many years[1-4]. The first experimental evidence of neutral interstellar hydrogen penetrating into the heliosphere was obtained from Lyman α sky background mapping[5,6]. Similar observations of interstellar helium using the He I 584-Å resonance line[7-9] revealed the existence of an interstellar neutral wind in interplanetary space which is subjected to the forces of solar gravitation and radiation pressure. When approaching the Sun, the interstellar gas is ionized by solar ultraviolet radiation, by charge exchange with solar wind ions and by collisions with solar wind electrons. The newly created ions are then picked up by the solar wind through interaction with the interplanetary magnetic field.

While most of the constituents are already ionized far beyond the orbit of the Earth, neutral helium (because of its high ionization potential) approaches the Sun to <1 AU (ref. 1). Therefore, a significant fraction of the helium is ionized inside the Earth's orbit and one would expect that these ions are observable by spacecraft in the solar wind. So far, no conclusive measurement on He^+ ions of interstellar origin has been given. Although signatures of He^+ in the solar wind with varying abundances have been reported occasionally[10,11], a systematic search for a permanently present flux of interstellar He^+ as part

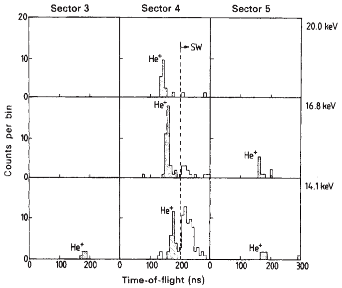

Fig. 1 Typical TOF-histograms at three different energy steps taken in the Sun sector and the two adjacent sectors. The data were obtained during a period of 45 min on 11 November 1984, at ~18 R_E in front of the Earth's bow shock.

Interstellar Pickup Ions

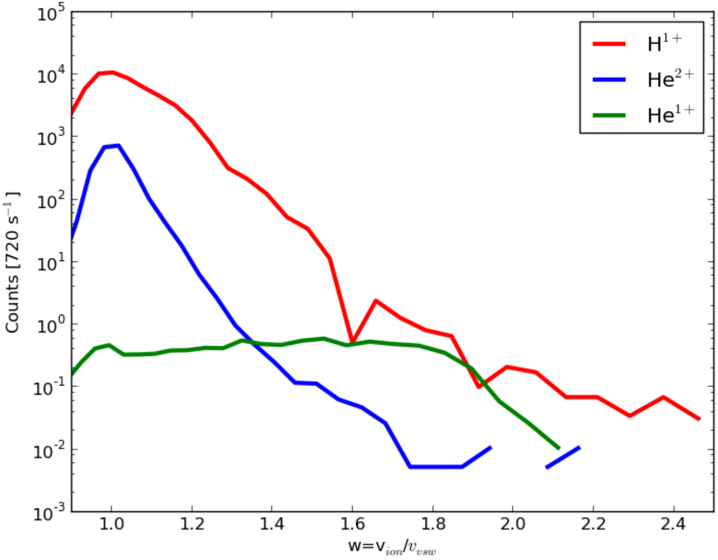

ACE/SWICS

Inner Source Pickup Ions

JOURNAL OF GEOPHYSICAL RESEARCH, VOL. 100, NO. A12, PAGES 23,373–23,377, DECEMBER 1, 1995

C^+ pickup ions in the heliosphere and their origin

J. Geiss,[1] G. Gloeckler,[2] L. A. Fisk,[3] and R. von Steiger[4,5]

Abstract. C^+ pickup ions were discovered with the solar wind ion composition spectrometer flying on Ulysses. Whereas the other nonlocally occurring pickup ions are produced from the interstellar gas penetrating deep into the heliosphere, C^+ comes from an "inner source" which is located at a solar distance of a few AU and extends over all heliospheric latitudes investigated so far. The total production of C^+, N^+, and O^+ by this inner source is of the order of 10^{-3} relative to the total production of O^+ from the interstellar gas in the heliosphere. Thus the inner source does not significantly contribute to oxygen or nitrogen in the anomalous cosmic rays (ACR), but its contribution to ACR carbon may not be negligible. We propose that the inner source material is carbon compounds evaporating from grains. At this time, the evidence points to interstellar grains as the major source, but we do not want to exclude yet a contribution from grains of solar system origin.

Inner Source - Velocity distributions

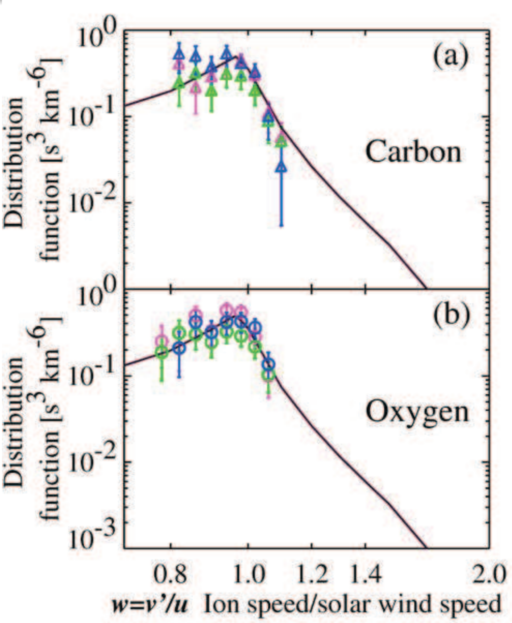

from Allegrini et al. 2005

Inner Source - Composition

Table 2. Element Abundance Ratios of the Inner Source PUIs Compared With Previous Results and to Solar Wind Abundances[a]

M/q (Element)	Inner Source: This Work	Inner Source: *Gloeckler et al.* [2000]	Solar Wind [*von Steiger et al.*, 2000]
$m/q = 12$ (C^+)	1.01 ± 0.12	1.46 ± 0.12	0.683 ± 0.040
$m/q = 14$ (N^+)	0.42 ± 0.07	0.40 ± 0.05	0.111 ± 0.022
$m/q = 16$ (O^+)	1.00 ± 0.10	1.00 ± 0.06	1 ± 0
$m/q = 20$ (Ne^+)	0.14 ± 0.03	0.32 ± 0.05	0.082 ± 0.013

[a]The inner source PUIs show a composition similar to solar wind composition.

from Allegrini et al. 2005

Inner Source - Extended Source

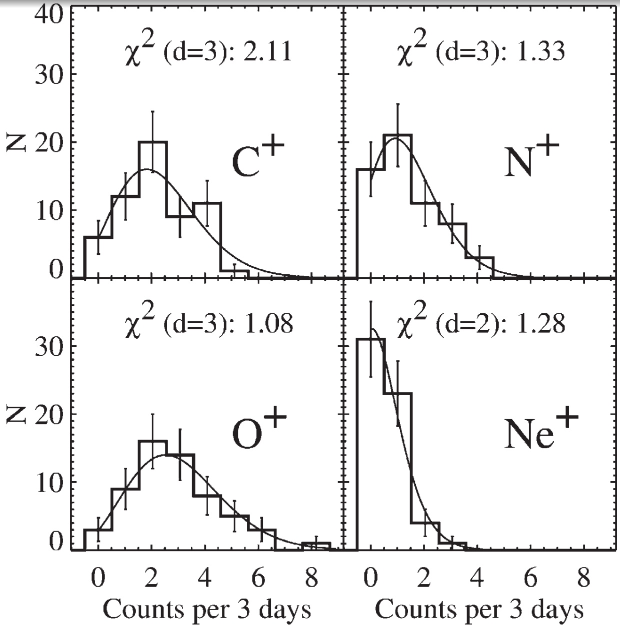

from Allegrini et al. 2005

Inner-source production scenarios

Sungrazing comets (Bzowski & Królikowska 2004)

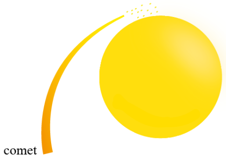

Dust-dust collisions (Mann & Czechowski 2005)

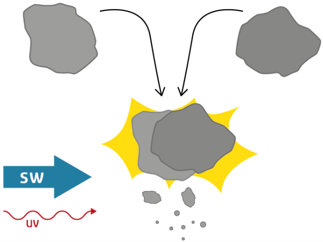

Solar wind recycling (Schwadron et al. 2000)

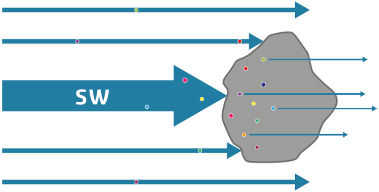

Solar wind neutralisation (Wimmer-Schweingruber & Bochsler 2003)

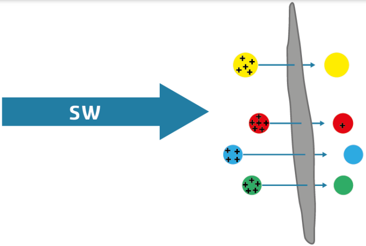

Inner-source production scenarios

A05105 ALLEGRINI ET AL.: BRIEF REPORT **A05105**

Table 3. Summary Table Listing the Proposed Mechanisms and Their Relation to the Five Constraints

	Scenario One, Solar Wind Recycling	Scenario Two, Solar Wind Neutralization	Scenario Three, Products of Sungrazing Comets	Scenario Four, Dust-Dust Collisions
Solar wind composition	Possibly[a]	Yes[b]	No[c]	No[c]
Peak near the Sun (10–30 R_S)	Yes	Yes	Possibly	Possibly
Large pickup ion flux	Unlikely[d]	Possibly	Possibly	Possibly
Randomly distributed source	Yes	Yes	Unlikely	Yes[e]
Stability over solar cycle	Yes	Unlikely[f]	Yes	Possibly

[a]Success of this scenario requires a very low sputtering yield.
[b]Grains act as carbon foils to neutralize the solar wind.
[c]Depleted in Ne, rich in C, Si, Mg, Fe.
[d]Grains efficiently scatter light and would yield a cross section 2 decades higher than observed from zodiacal light.
[e]However, peaks at low latitude.
[f]Success of this scenario requires that CMEs do not trap nanometer-sized grains.

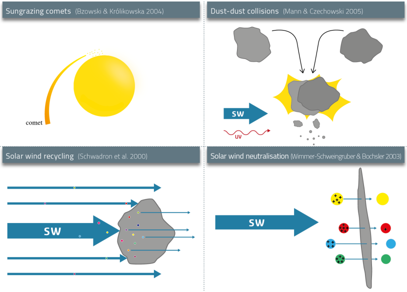

Heavy Pickup Ions - CTOF Observations

CTOF - m/q Spectra

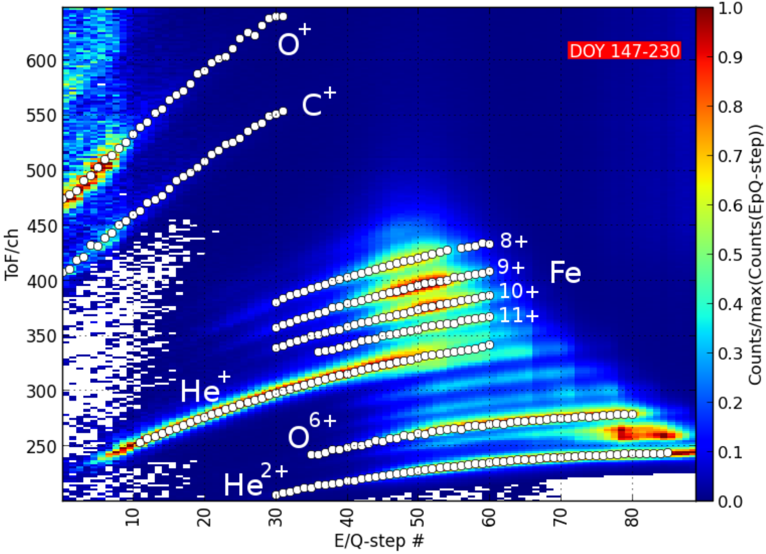

CTOF - m/q Spectra

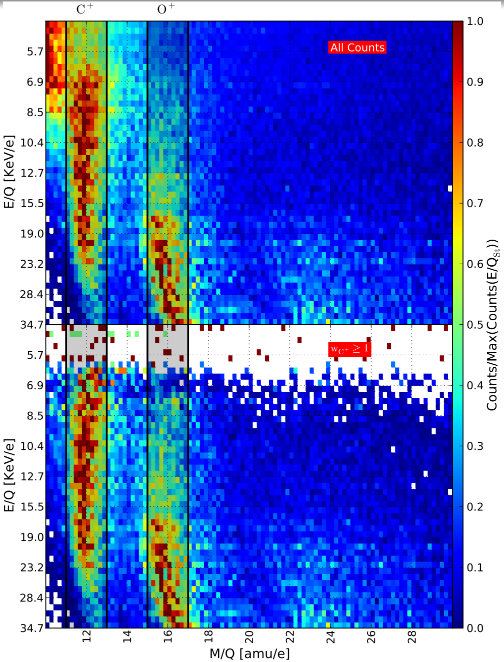

Inner Source Pickup Ions - CTOF

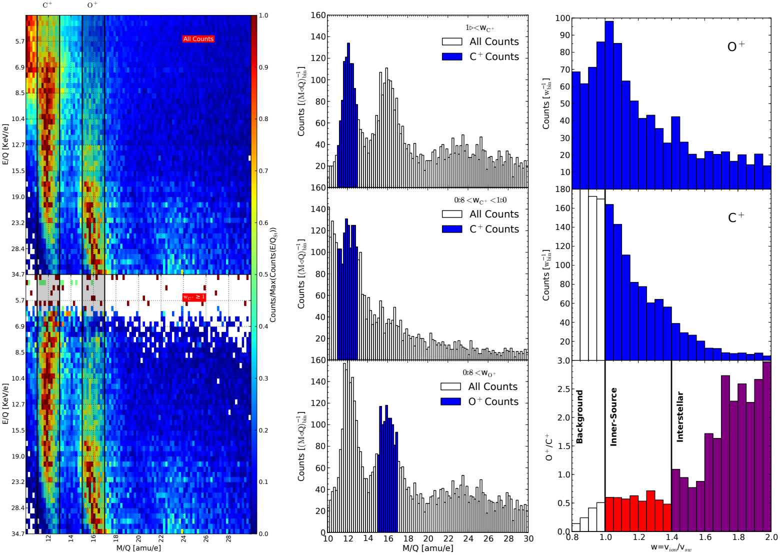

from Berger et al. 2013

Correlation of Inner-Source and Solar-Wind flux?

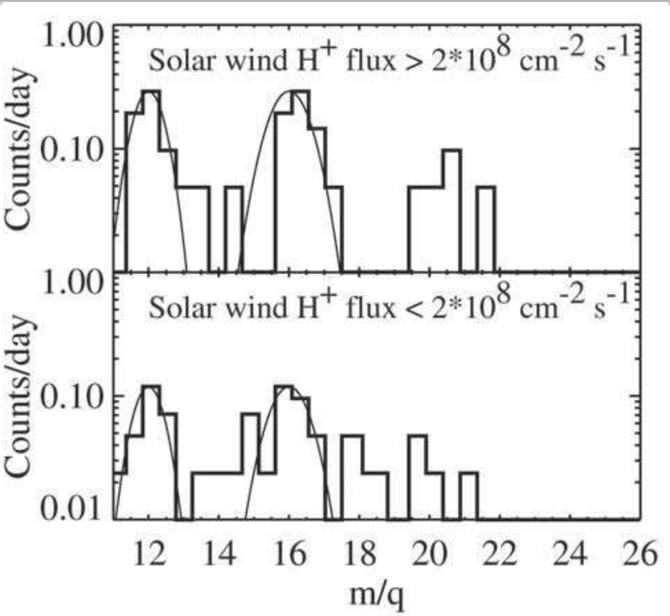

from Allegrini et al. 2005

CTOF - Observations

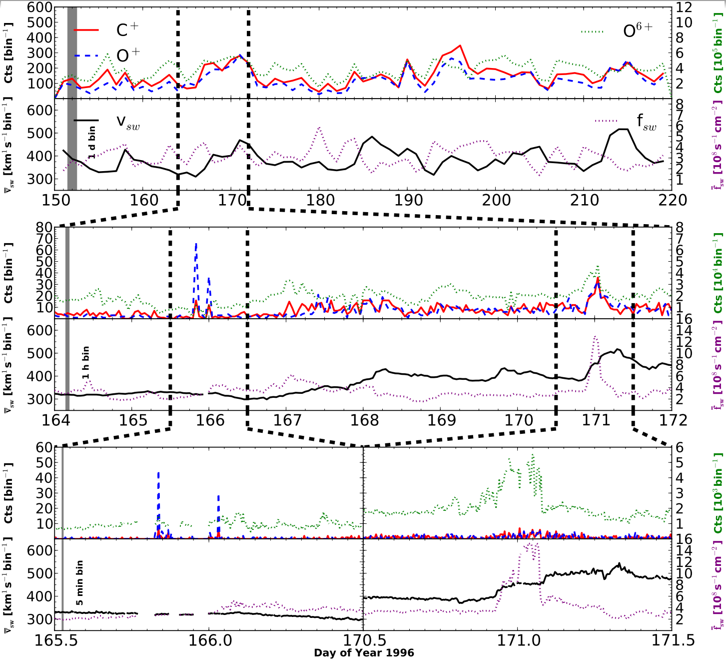

CTOF - Statistics

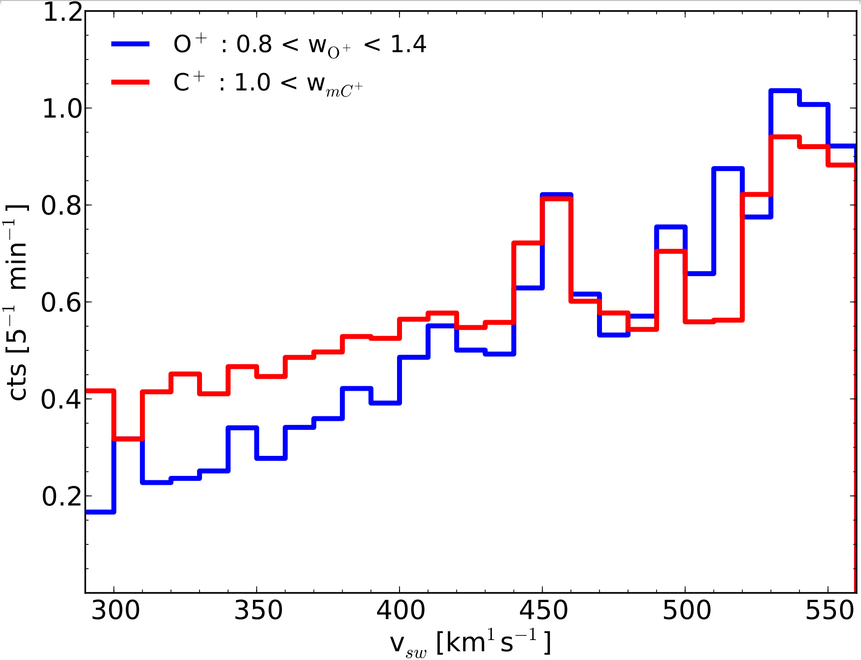

Variability

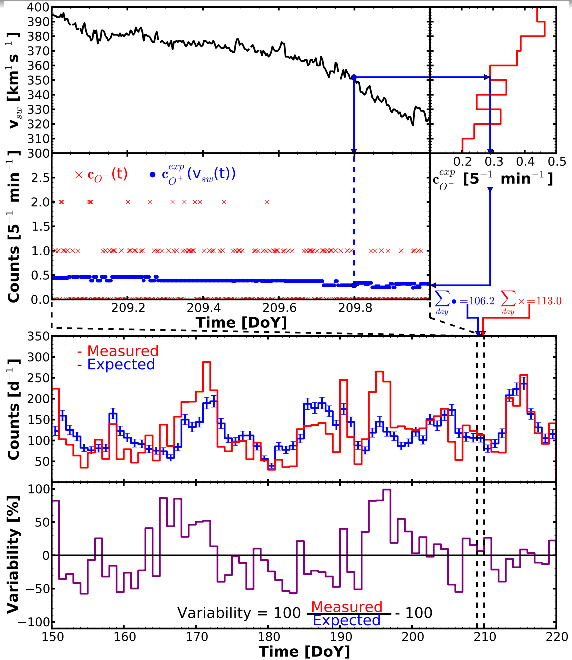

Correlations

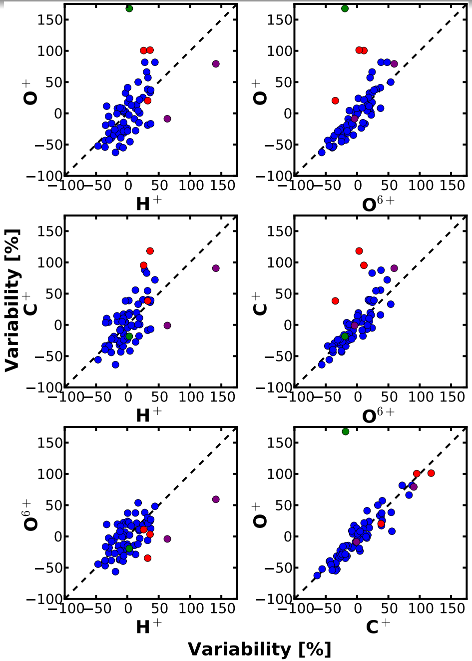

Correlations - Cadence

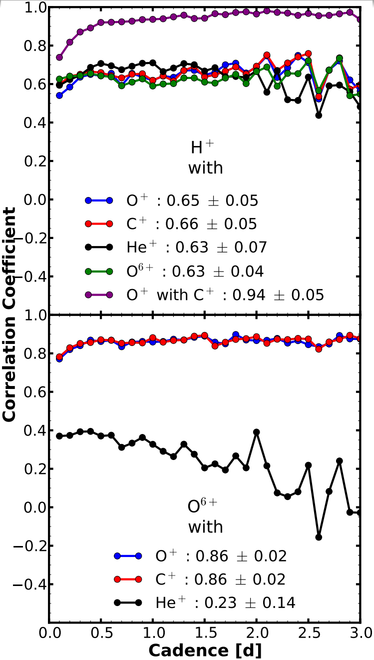

Correlations - Periods

	T1		T2	
	H^+	O^{6+}	H^+	O^{6+}
O^+	0.61 ± 0.04	0.76 ± 0.04	0.65 ± 0.05	0.86 ± 0.02
C^+	0.64 ± 0.03	0.74 ± 0.04	0.66 ± 0.05	0.86 ± 0.02
He^+	0.70 ± 0.07	0.26 ± 0.12	0.63 ± 0.07	0.23 ± 0.14
O^{6+}	0.53 ± 0.07	-	0.63 ± 0.04	-

	O^+ T1	O^+ T2
C^+	0.95 ± 0.04	0.94 ± 0.05

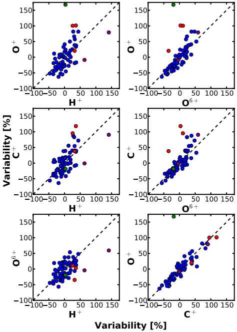

Inner-source PUI composition

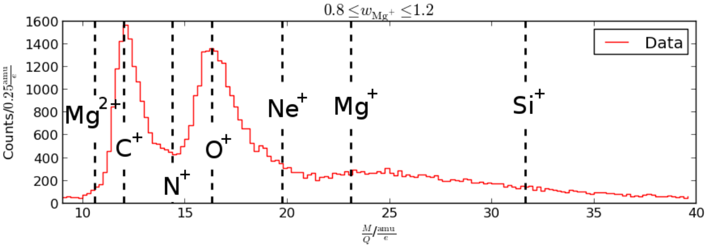

- M/Q resolution and large geometry factor should be sufficient to derive C^+, N^+, O^+, Ne^+, Mg^+, Mg^{2+}, and Si^+ abundance ratios.
- Inner-source PUIs dominate in $0.8 \leq w \leq 1.2$.
- Statistical assignment of counts!

Inner-source PUI composition

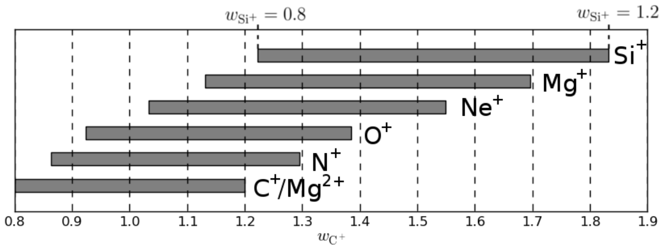

- Sort counts by w_{C^+}.
- Fit M/Q histograms, take efficiency into account.
- Compose total flux by accumulating over the w-range.

Peak shape model

$$f\left(\frac{M}{Q}\right) = A_0 \cdot \begin{cases} \exp\left(-\frac{\left(\frac{M}{Q}-\frac{M}{Q}_0\right)^2}{2\sigma_l^2}\right) & \text{if} \quad \frac{\mathrm{M}}{\mathrm{Q}} \leq \frac{\mathrm{M}}{\mathrm{Q}}_0 \\ \left(1-\frac{\left(\frac{M}{Q}-\frac{M}{Q}_0\right)^2}{\kappa_r\sigma_r^2}\right)^{-\kappa_r} & \text{if} \quad \frac{\mathrm{M}}{\mathrm{Q}} > \frac{\mathrm{M}}{\mathrm{Q}}_0 \end{cases}$$

- Derived ratios for σ_l, σ_r, and κ_r between all ion species from TRIM simulations.
  $\rightarrow$ κ_r fixed; one parameter for σ_l and σ_r to describe all ion distributions!
- Fit of the M/Q histograms with resampling using Poisson noise.
  $\rightarrow$ Functions $\sigma_l(E_{post})$ and $\sigma_r(E_{post})$.

M/Q Fits

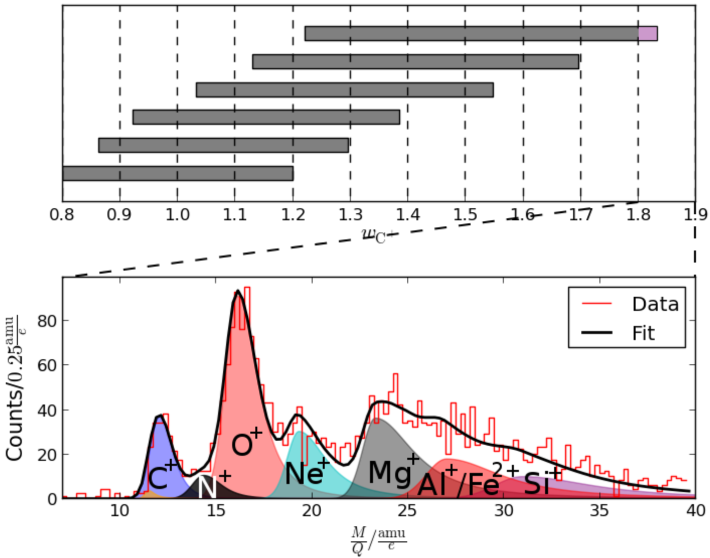

0.8
0.9
1.0
1.1
1.2
1.3
1.4
1.5
1.6
1.7
1.8
1.9
w_{C^+}
Counts/$0.25\frac{\text{amu}}{e}$
0
20
40
60
80
Data
Fit
C^+
N^+
O^+
Ne^+
Mg^+
Al^+/Fe^{2+}
Si^+
10
15
20
25
30
35
40
$\frac{M}{Q}/\frac{\text{amu}}{e}$

M/Q Fits

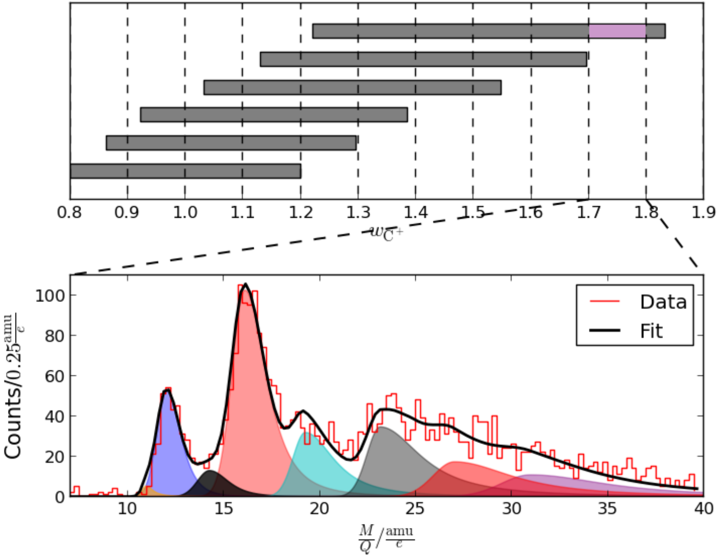
0.8
0.9
1.0
1.1
1.2
1.3
1.4
1.5
1.6
1.7
1.8
1.9
w_{C^+}
Data
Fit
Counts/$0.25\frac{amu}{e}$
0
20
40
60
80
100
10
15
20
25
30
35
40
$\frac{M}{Q}/\frac{amu}{e}$

M/Q Fits

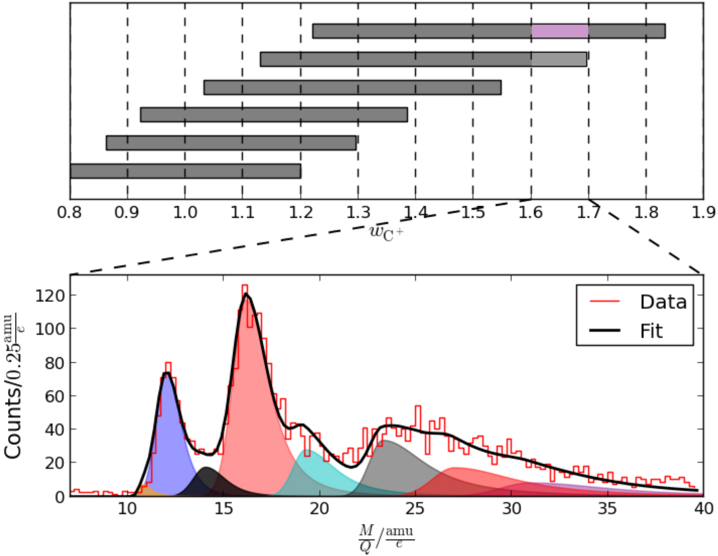

0.8
0.9
1.0
1.1
1.2
1.3
1.4
1.5
1.6
1.7
1.8
1.9
w_{C^+}
Data
Fit
Counts/0.25$\frac{amu}{e}$
0
20
40
60
80
100
120
10
15
20
25
30
35
40
$\frac{M}{Q}/\frac{amu}{e}$

M/Q Fits

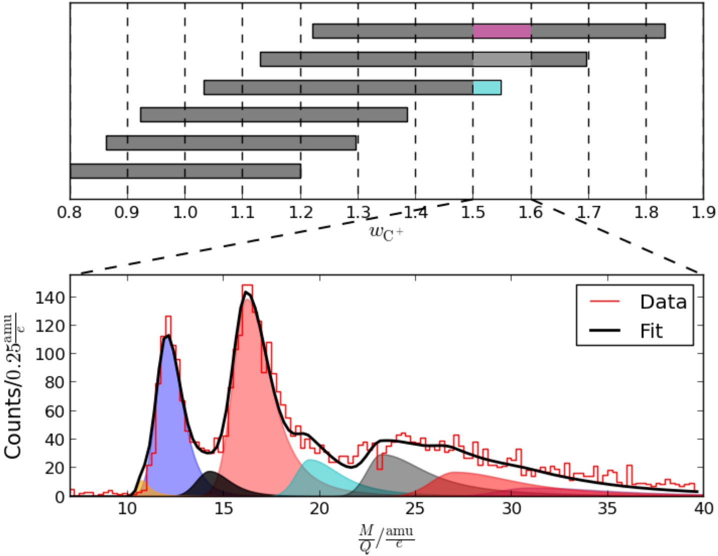

0.8
0.9
1.0
1.1
1.2
1.3
1.4
1.5
1.6
1.7
1.8
1.9
w_{C^+}
Counts/$0.25\frac{amu}{e}$
140
120
100
80
60
40
20
0
Data
Fit
10
15
20
25
30
35
40
$\frac{M}{Q}/\frac{amu}{e}$

M/Q Fits

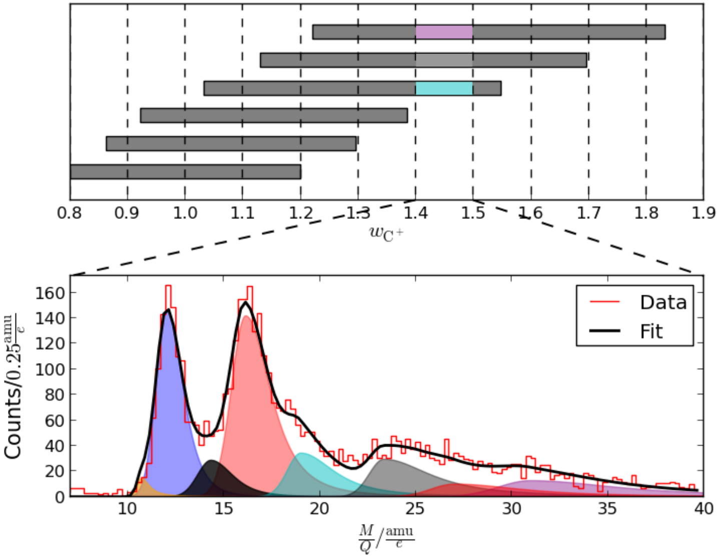

0.8 0.9 1.0 1.1 1.2 1.3 1.4 1.5 1.6 1.7 1.8 1.9
w_{C^+}
Data
Fit
Counts/$0.25\frac{\text{amu}}{e}$
0 20 40 60 80 100 120 140 160
10 15 20 25 30 35 40
$\frac{M}{Q}/\frac{\text{amu}}{e}$

M/Q Fits

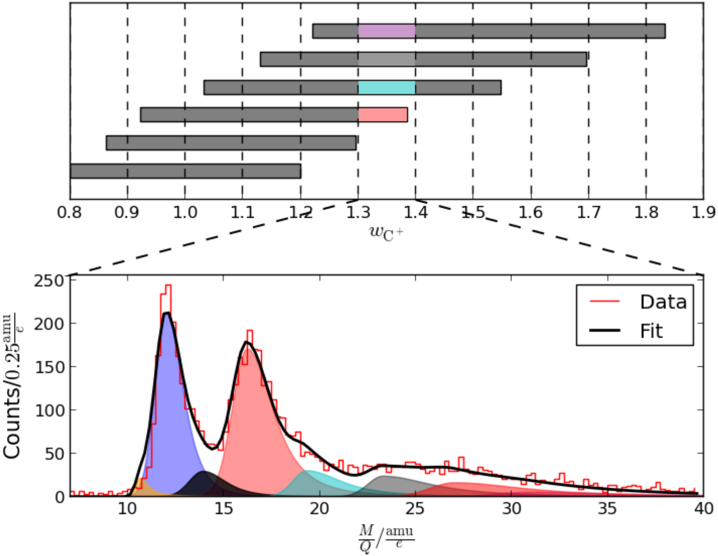

0.8
0.9
1.0
1.1
1.2
1.3
1.4
1.5
1.6
1.7
1.8
1.9
w_{C^+}
250
200
150
100
50
0
Counts/0.25$\frac{amu}{e}$
10
15
20
25
30
35
40
$\frac{M}{Q}/\frac{amu}{e}$
Data
Fit

M/Q Fits

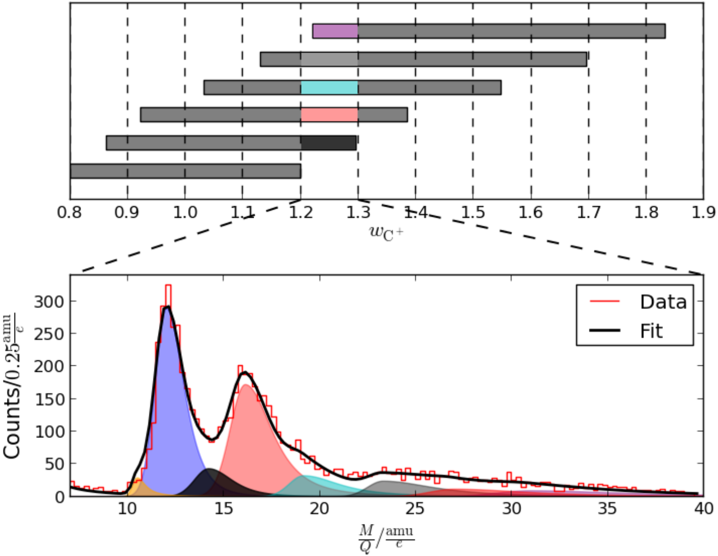

0.8
0.9
1.0
1.1
1.2
1.3
1.4
1.5
1.6
1.7
1.8
1.9
w_{C^+}
Data
Fit
Counts/$0.25\frac{\text{amu}}{e}$
0
50
100
150
200
250
300
10
15
20
25
30
35
40
$\frac{M}{Q}/\frac{\text{amu}}{e}$

M/Q Fits

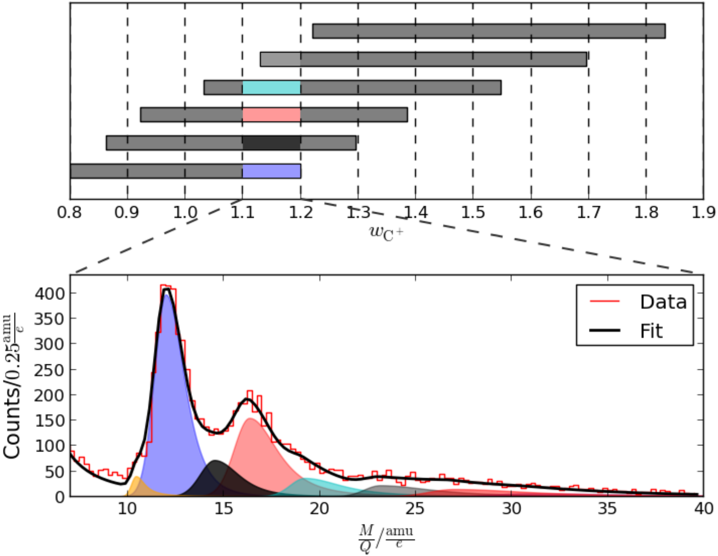

0.8
0.9
1.0
1.1
1.2
1.3
1.4
1.5
1.6
1.7
1.8
1.9
w_{C^+}
Data
Fit
400
350
300
250
200
150
100
50
0
Counts/$0.25\frac{amu}{e}$
10
15
20
25
30
35
40
$\frac{M}{Q}/\frac{amu}{e}$

M/Q Fits

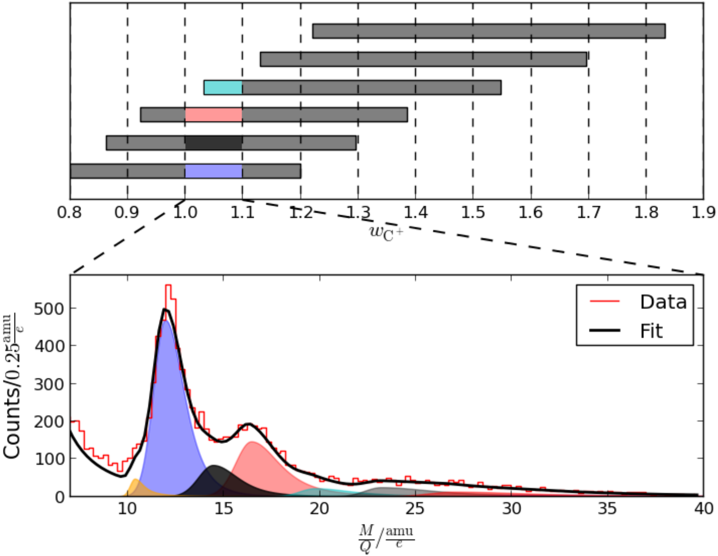

0.8
0.9
1.0
1.1
1.2
1.3
1.4
1.5
1.6
1.7
1.8
1.9
w_{C^+}
Data
Fit
Counts/0.25$\frac{amu}{e}$
500
400
300
200
100
0
10
15
20
25
30
35
40
$\frac{M}{Q}/\frac{amu}{e}$

M/Q Fits

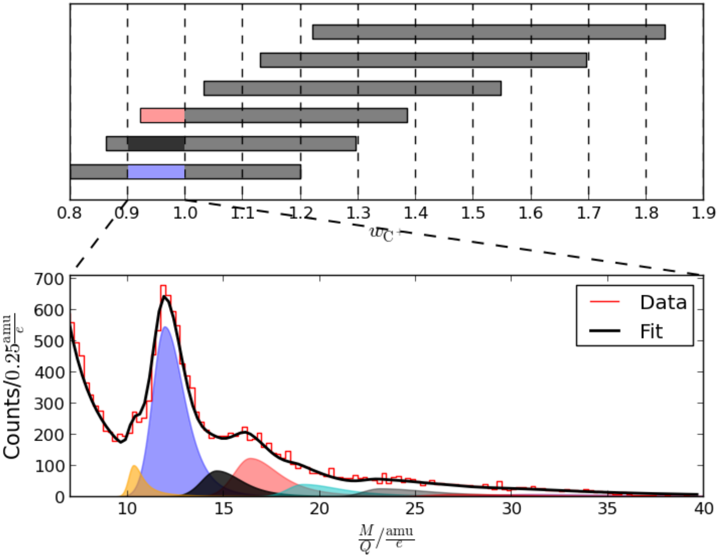
0.8
0.9
1.0
1.1
1.2
1.3
1.4
1.5
1.6
1.7
1.8
1.9
w_{C^+}
700
600
500
400
300
200
100
0
Counts/0.25$\frac{amu}{e}$
10
15
20
25
30
35
40
$\frac{M}{Q}/\frac{amu}{e}$
Data
Fit

M/Q Fits

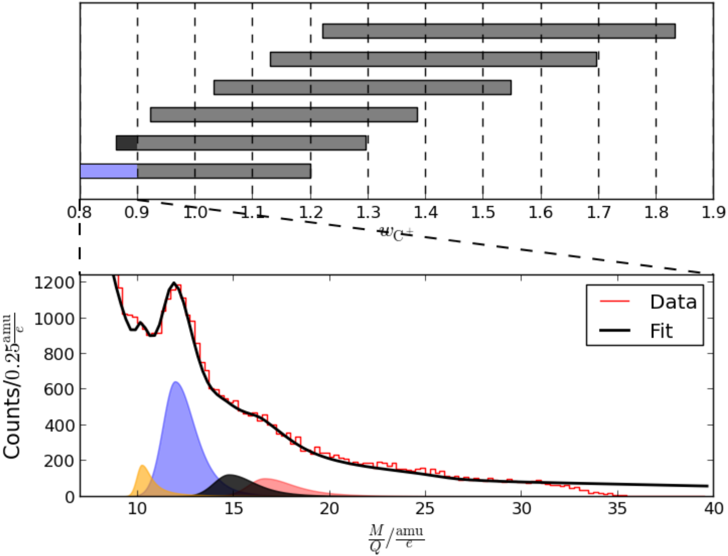

0.8
0.9
1.0
1.1
1.2
1.3
1.4
1.5
1.6
1.7
1.8
1.9
w_{C^+}
1200
1000
800
600
400
200
0
10
15
20
25
30
35
40
Counts/0.25$\frac{amu}{e}$
$\frac{M}{Q}/\frac{amu}{e}$
Data
Fit

Efficiency

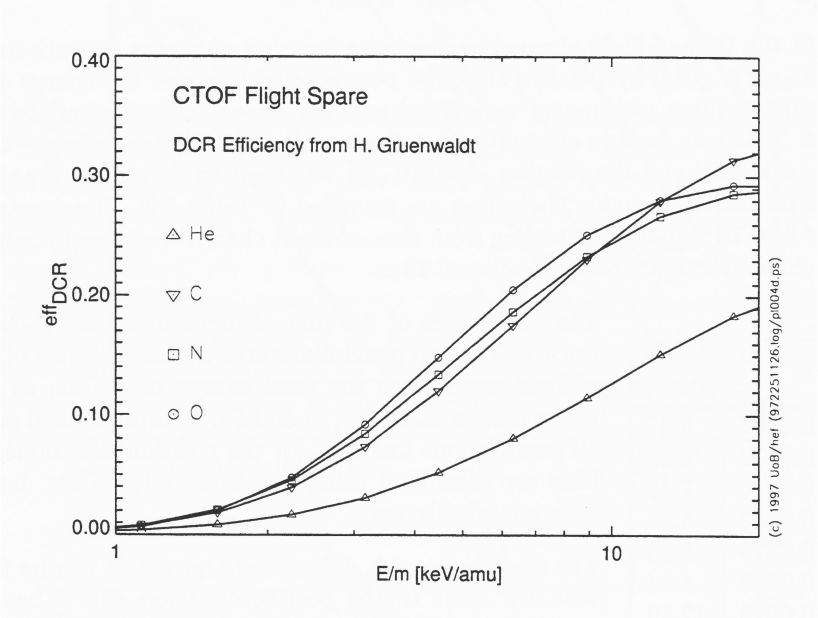
CTOF Flight Spare
DCR Efficiency from H. Gruenwaldt
He
C
N
O
0.40
0.30
0.20
0.10
0.00
eff_DCR
1
10
E/m [keV/amu]
(c) 1997 UoB/hef (97225112 6.log/pl004d.ps)

Efficiency

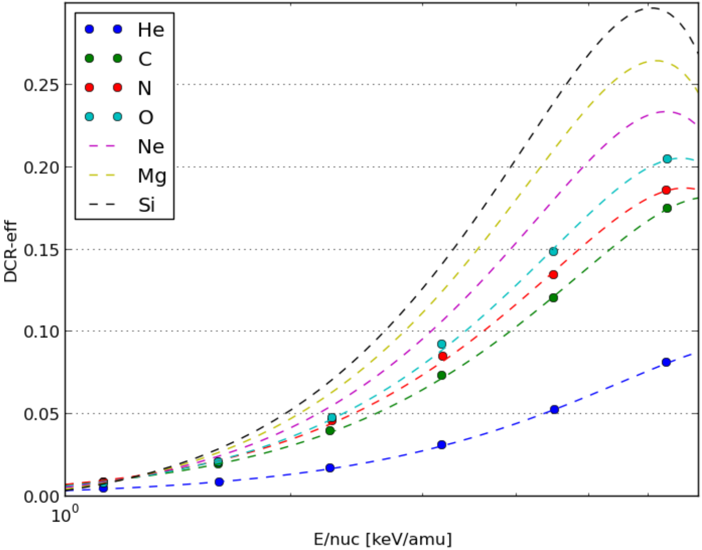

Results

Ion	$M/Q/\frac{\text{amu}}{e}$	$\frac{\text{Ion}}{\text{C}^+}$	Solar Wind (von Steiger et al. 2000)
C^+	12	$\equiv 1$	$\equiv 1$
N^+	14	0.22 ± 0.03	0.13 ± 0.04
O^+	16	0.57 ± 0.04	1.49 ± 0.19
Ne^+	20	0.19 ± 0.01	0.16 ± 0.04
Mg^+	24	0.30 ± 0.01	0.21 ± 0.09
Mg^{2+}	12	0.07 ± 0.01	
Si^+	28	0.21 ± 0.02	0.20 ± 0.07

Simulation

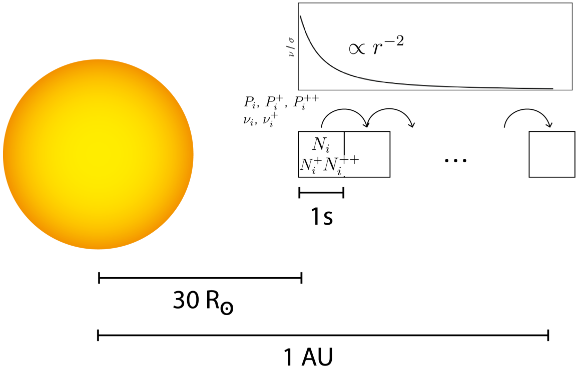

- Production rates due to ion-dust interaction P_i, P_i^+, and P_i^{++}; cross-section $\sigma \propto r^{-2}$
- Photo-ionisation rates ν and ν^+.

Simulation

Ion	$M/Q/\frac{\text{amu}}{e}$	$\frac{\text{Ion}}{\text{C}^+}$	Simulation
C^+	12	$\equiv 1$	$\equiv 1$
N^+	14	0.22 ± 0.03	0.07 ± 0.03
O^+	16	0.57 ± 0.04	0.59 ± 0.08
Ne^+	20	0.19 ± 0.01	0.05 ± 0.02
Mg^+	24	0.30 ± 0.01	0.28 ± 0.11
Mg^{2+}	12	0.07 ± 0.01	0.05 ± 0.02
Si^+	28	0.21 ± 0.02	0.43 ± 0.09
Si^{2+}	14	-	0.05 ± 0.01

Simulation

Ion	$M/Q/\frac{\text{amu}}{e}$	$\frac{\text{Ion}}{\text{C}^+}$	Simulation
C^+	12	$\equiv 1$	$\equiv 1$
$(N^+ + Si^{2+})^*$	14	0.14 ± 0.03	0.12 ± 0.04
O^+	16	0.57 ± 0.04	0.59 ± 0.08
Ne^+	20	0.19 ± 0.01	0.05 ± 0.02
Mg^+	24	0.30 ± 0.01	0.28 ± 0.11
Mg^{2+}	12	0.07 ± 0.01	0.05 ± 0.02
Si^+	28	0.21 ± 0.02	0.43 ± 0.09

*50% of counts N^+, 50% of counts Si^{2+}

Results

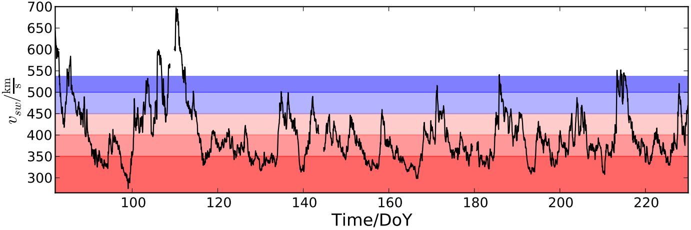

Solar wind speed$/\frac{\text{km}}{\text{s}}$	$\frac{O^+}{C^+}$
≤ 350	0.52 ± 0.04
$350 - 400$	0.57 ± 0.07
$400 - 450$	0.66 ± 0.07
$450 - 500$	0.87 ± 0.10
$500 - 537$	0.96 ± 0.17

Possible reasons

- Production rates depend on solar wind speed in the solar wind neutralization scenario.

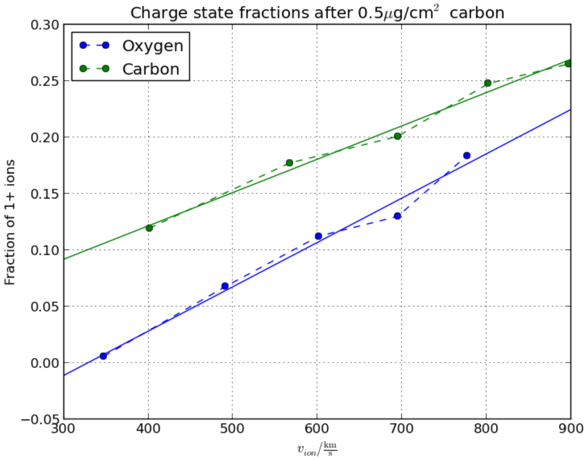

Possible reasons

- Production rates depend on solar wind speed in the solar wind neutralization scenario.
- Different charge-exchange ionisation cross-sections and/or differential streaming.
- Solar wind elemental composition changes with solar wind speed?
- Instrumental effects?

Summary

CTOF heavy PUI observations:

- The inner-source heavy PUI flux is correlated with the solar wind heavy ion flux.
- The measured inner-source heavy PUI composition can be explained with the solar wind neutralization production scenario.
- The O^+/C^+ abundance ratio increases systematically with increasing solar wind speed.